THE JOURNAL OF BIOLOGICAL CHEMISTRY VOL. 291, NO. 34, pp. 17816–17828, August 19, 2016

Monooxygenase Substrates Mimic Flavin to Catalyze Cofactorless Oxygenations*

Received for publication, March 29, 2016, and in revised form, June 8, 2016 Published, JBC Papers in Press, June 15, 2016, DOI 10.1074/jbc.M116.730051

Melodie M. Machovina, Robert J. Usselman, and Jennifer L. DuBois[1]

From the Department of Chemistry and Biochemistry, Montana State University, Bozeman, Montana 59715-3400

Members of the antibiotic biosynthesis monooxygenase family catalyze O_2-dependent oxidations and oxygenations in the absence of any metallo- or organic cofactor. How these enzymes surmount the kinetic barrier to reactions between singlet substrates and triplet O_2 is unclear, but the reactions have been proposed to occur via a flavin-like mechanism, where the substrate acts in lieu of a flavin cofactor. To test this model, we monitored the uncatalyzed and enzymatic reactions of dithranol, a substrate for the nogalamycin monooxygenase (NMO) from *Streptomyces nogalater*. As with flavin, dithranol oxidation was faster at a higher pH, although the reaction did not appear to be base-catalyzed. Rather, conserved asparagines contributed to suppression of the substrate pK_a. The same residues were critical for enzymatic catalysis that, consistent with the flavoenzyme model, occurred via an O_2-dependent slow step. Evidence for a superoxide/substrate radical pair intermediate came from detection of enzyme-bound superoxide during turnover. Small molecule and enzymatic superoxide traps suppressed formation of the oxygenation product under uncatalyzed conditions, whereas only the small molecule trap had an effect in the presence of NMO. This suggested that NMO both accelerated the formation and directed the recombination of a superoxide/dithranyl radical pair. These catalytic strategies are in some ways flavin-like and stand in contrast to the mechanisms of urate oxidase and (1*H*)-3-hydroxy-4-oxoquinaldine 2,4-dioxygenase, both cofactor-independent enzymes that surmount the barriers to direct substrate/O_2 reactivity via markedly different means.

Reactions between organic molecules and O_2 are among the most important in biology, powering aerobic life. These reactions also present a distinct mechanistic challenge, as O_2 has two unpaired electrons ($^3O_2$, ↑ ↑), although most organic substrates (S) have all their spins paired (^1S, ↑ ↓). Uncatalyzed reactions between the two violate the so-called spin rule and are consequently slow (1). The sluggishness of these reactions protects biological organisms from potentially destructive oxidations and necessitates the use of catalysts for activating and directing O_2 reactivity.

Enzyme-associated cofactors, flavins, pterins, or redox-active metals that are capable of sequentially donating electrons to O_2, provide a pathway of microscopic chemical steps, each of which adheres to the spin rule. Cofactors have therefore long been assumed to serve an obligate role in the catalytic activation of O_2 in biological systems. Over the last 2 decades, however, O_2-activating enzymes that defy chemical expectation by not requiring cofactors have been discovered (2). These enzymes are biologically diverse, coming from several structural classes and evolutionary families and deriving from all kingdoms of life. They act upon a variety of substrates that nonetheless tend to be highly conjugated good reducing agents. Because they use O_2 from air, they require no exogenous metals or redox-sensitive organic components, and they have all of the benefits of biocatalysis, cofactor-free oxidases and oxygenases provide a model for "green" oxidation chemistry.

In part because of the nature of their substrates, the O_2-activating mechanisms of many cofactor-independent oxygenases have been proposed to be flavoprotein-like (3–8). Flavoprotein-dependent oxidases and oxygenases are able to accelerate the rate of the flavin/O_2 reaction by 10^4–10^6-fold over the reaction of free flavin in aqueous solution (9, 10) according to principles that are well described (summarized in Scheme 1). The flavin acts as an intermediary, activating O_2 and using it either to hydroxylate an exogenous substrate or to dispose of substrate-derived electrons (as H_2O_2). In the cofactor-free enzymes, the substrate itself has been proposed to reductively activate O_2 via the same series of steps used by the flavin cofactor. The activated substrate-O_2 complex subsequently converts to the oxidized product. Such a motivating model, although plausible, has not been widely tested.

The antibiotic biosynthesis monooxygenase family (ABMs,[2] Pfam family PF03992) contains several small, structurally simple, and intrinsically solvent- and temperature-stable enzymes known to catalyze O_2-dependent and cofactor-independent oxidations or monooxygenations (5–8, 11–15). Many ABMs are part of the biosynthetic pathways for polyketide antibiotics, including tetracenomycin (14, 16), daunomycin (17), actinorhodin (8, 12), alnumycin (18), and aclacinomycin (11), also known as nogalamycin (19). Additionally, a subset of ABMs

* This work was supported by startup funding from Montana State University. The authors declare that they have no conflicts of interest with the contents of this article. The content is solely the responsibility of the authors and does not necessarily represent the official views of the National Institutes of Health.

[1] To whom correspondence should be addressed: Dept. of Chemistry and Biochemistry, 221 Chemistry and Biochemistry Bldg., Montana State University, Bozeman, MT 59715-3400. Tel.: 406-994-2844; Fax: 406-994-5407; E-mail: jdubois@chemistry.montana.edu.

[2] The abbreviations used are: ABM, antibiotic biosynthesis monooxygenase; NMO, nogalamycin monooxygenase; CMH, 1-hydroxy-3-methoxycarbonyl-2,2,5,5-tetramethylpyrrolidine; HOD, (1*H*)-3-hydroxy-4-oxoquinaldine 2,4-dioxygenase; ME, 2-methoxyethanol; TEMPO, 2,2,6,6-tetramethyl-1-piperidinyloxy; SOD, superoxide dismutase; Tricine, *N*-[2-hydroxy-1,1-bis(hydroxymethyl)ethyl]glycine; CAPS, 3-(cyclohexylamino)propanesulfonic acid; CHES, 2-(cyclohexylamino)ethanesulfonic acid; BES, 2-[bis(2-hydroxyethyl)amino]ethanesulfonic acid.

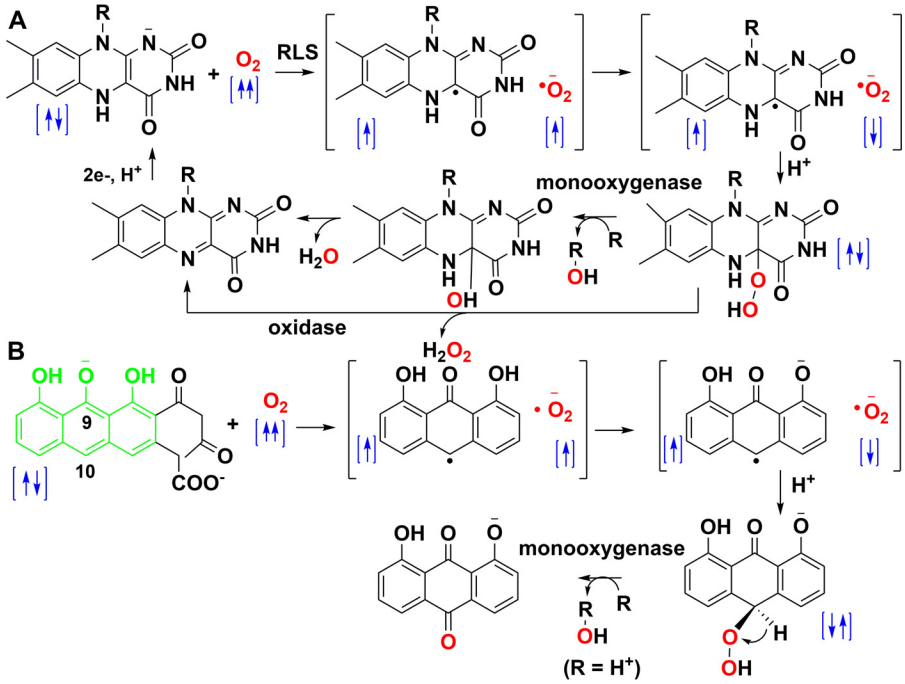

SCHEME 1. **Flavin/O_2 reaction scheme (*A*) and analogous reaction pathway for NMO (*B*).** *A,* in the initial step of the reaction, the reduced, deprotonated flavin anion transfers one electron to triplet-state O_2 to form a superoxide (↑)/semiquinone (↑) radical pair (9, 10, 56–58). This spin-allowed step is rate-limiting in several flavin-oxidases and -oxygenases (59). Deprotonation of both the flavin and, in monooxygenases, the organic substrate occurs, the latter in a base-catalyzed manner (35, 36, 60). The presence of an active site positive charge lowers the height of the activation barrier in some well studied flavoproteins (37) by stabilizing the superoxide anion and helping to minimize the electron transfer reorganization energy (λ) (38, 39). The reaction between the superoxide/semiquinone radical pair to form the C4a-flavin-hydroperoxide (*C4a-OOH*) intermediate is enforced via site isolation, which prevents autocatalytic reactions between the oxidized and reduced flavins to form semiquinones (10). The C4a-OOH releases H_2O_2 to form the two-electron-oxidized flavin in flavin-dependent oxidases. Alternatively, the terminal oxygen may be transferred to a substrate in a flavin-dependent monooxygenase (36). *B,* analogous mechanism for NMO is proposed. The native 1,2-nogalonate substrate is shown, with the dithranol anion core highlighted in *green*.

known as IsdGs catalyze the ring-opening oxygenation of the metallosubstrate heme (20) in many heme-feeding pathogenic bacteria.

Here, we have tested three essential components of the flavin model for the reaction catalyzed by the cofactor-independent nogalamycin monooxygenase (NMO), an ABM from *Streptomyces nogalater* (gene locus, SnoaB). We have compared the properties of the reaction in both the presence and absence of the enzyme to understand how the latter contributes to catalysis. Finally, we have interpreted the results in light of mechanistic work with IsdG (from *Staphylococcus aureus*) (21) and the emerging model for catalysis by the increasingly well characterized cofactor-independent oxygenase, (1*H*)-3-hydroxy-4-oxoquinaldine 2,4-dioxygenase (HOD) (4, 22–27).

Results

Characterization of the Enzyme, Substrate, and Products—His_6-NMO was purified in yields of ~25 mg/liter culture. Pure enzyme had a measured subunit molecular mass of 16.85 kDa (MS); calculated 16.98 kDa. The discrepancy was attributed to loss of part of the histidine tag before or during MS analysis. The enzyme retained full activity for at least 25 min in the ME-containing buffers, after which activity began to decline.

UV-visible spectra for dithranol were monitored as a function of pH (Fig. 1*A*). Plots of absorbance at 354 and 389 nm *versus* pH yielded sigmoidal curves that were fit to Equation 3, yielding an average $pK_a = 8.5 \pm 0.3$ (Fig. 1*A*, *inset*), ascribed to the conversion of neutral dithranol to the monoanionic enolate (dithranolate) (Scheme 2) (28). UV-visible features were identified under acidic and alkaline conditions in the buffer/ME solvent (Fig. 1*B*). Well resolved HPLC peaks for dithranol and its oxidation products were obtained with retention times of 5.9 min (dithranol), 5.2 min (dithranone), and 8.5 min (bisanthrone) (data not shown).

Uncatalyzed Oxidation of Dithranol in Air—The spontaneous conversion of dithranol to products was monitored in air (280 μM O_2) >2 units below dithranol's pK_a (pH 6.3) via time-resolved UV-visible spectroscopy. The dithranol peak maximum red-shifted over a period of hours to 392 nm as the yellow starting solution turned brown (Fig. 2*A*). The lack of isosbestic behavior was consistent with the formation of more than one product. The reaction was subsequently monitored over time by discontinuous HPLC ($[\text{dithranol}]_{\text{initial}} = 500\ \mu$M, Fig. 2*B*). The curve indicating the progress of reaction for dithranol disappearance fit well to a single exponential equation, yielding $k = 0.0028 \pm 0.0001\ \text{min}^{-1}$ ($t_{½} = 240$ min, see Table 1). This exactly matched the first-order rate of bisanthrone formation. The major product (90%) was bisanthrone, with 10% dithranone (HPLC quantification errors were ≤10%).

The same reactions were subsequently monitored for the alkaline form of dithranol (pH 9.8, Fig. 3*A*). The dithranol peak (389 nm) red-shifted over a period of minutes to a product spectrum closely resembling that of dithranone. Dithranolate disappearance monitored by HPLC (500 μM) was linear with time and significantly faster than under acidic conditions (20

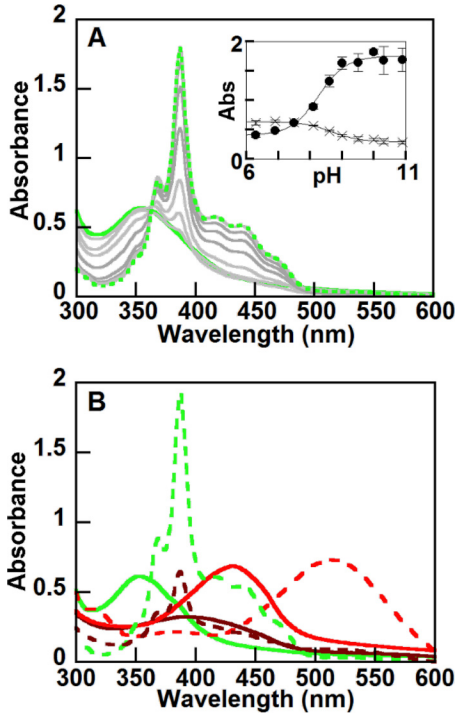

FIGURE 1. **Substrate (dithranol) and its oxidation products have distinct spectra.** *A,* titration of 0.5 ml of 100 μM dithranol in Tris-ME with 5 M NaOH (1 μl), illustrating changes in the spectrum as the pH is increased from 5 (*solid green trace*) to 11 (*dashed green trace*). Spectra measured at intervening increments of NaOH are shown in *gray*. *Inset,* absorbance at 354 nm (×) and 387 nm (●) as a function of pH. The data were fit to Equation 3 ($pK_a = 8.5 \pm 0.30$). *B,* UV-visible spectra of dithranol (*green*), bisanthrone (*brown*), and dithranone (*red*), at 100 μM (pH 6.3) (0.1 M citrate/ME (pH 6.3)). Spectra for the same species measured under alkaline conditions (0.1 M CAPS/ME (pH 9.8)) are shown in the same colors as *dashed lines*. Measured acidic features were as follows: dithranol $\lambda_{max} = 354$ nm and $\epsilon_{354\ nm} = 6.5\ (\pm 0.2)\ mM^{-1}cm^{-1}$; dithranone, $\lambda_{max} = 430$ nm, $\epsilon_{430\ nm} = 7.3\ (\pm 0.02)\ mM^{-1}\ cm^{-1}$; and bisanthrone, $\lambda_{max} = 392$ nm. Features for the alkaline species were as follows: dithranol $\lambda_{max} = 389$ nm, $\epsilon_{389\ nm} = 18\ (\pm 0.2)\ mM^{-1}\ cm^{-1}$; dithranone $\lambda_{max} = 512$ nm, $\epsilon_{512\ nm} = 6.6\ (\pm 0.06)\ mM^{-1}\ cm^{-1}$; and bisanthrone $\lambda_{max} = 387$ nm.

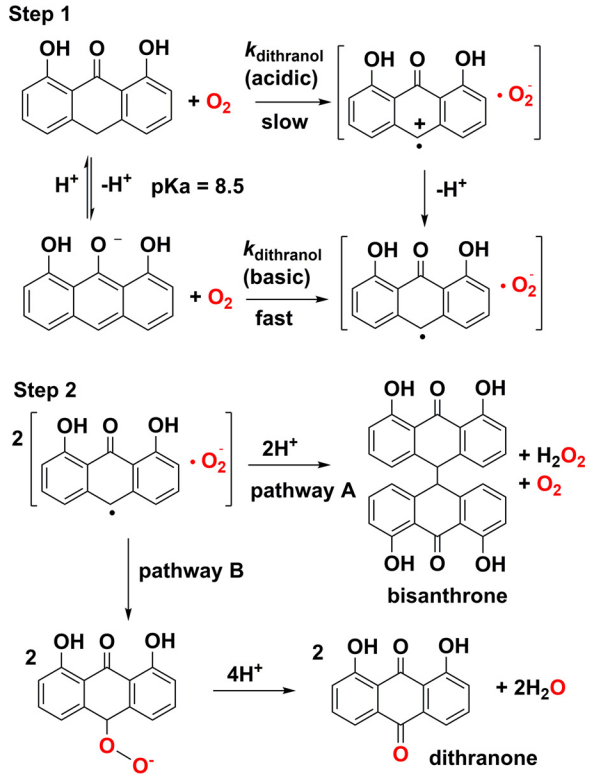

SCHEME 2. **Proposed pathways for the uncatalyzed oxidation of dithranol.** Step 1 results in formation of a dithranyl/superoxide radical pair. In Step 2, the radical pair may dissociate, resulting in dimerization of two dithranyls to form bisanthrone. The expected rapid disproportionation of two superoxide radicals to form H_2O_2 and O_2 is also shown (*pathway A*). Alternatively, the radical pair can combine (*pathway B*), forming the peroxy adduct. Heterolytic cleavage of the O–O bond leads to water and dithranone. Pathway A predominates under acidic conditions and pathway B under basic conditions.

(± 1) μM min^{-1}, see Fig. 3*B* and Table 1), converting to a mixture of the alkaline forms of dithranone (60%) and bisanthrone (40%). The shift to an apparent zero-order reaction (in dithranol) was observed when $[dithranol]_{initial} > [O_2]$ and appeared to result from the rapid depletion of O_2 relative to the rate of re-equilibration of the solution with air. When the reaction was carried out at $[dithranol]_{initial} = 30$ μM, the dithranol *versus* time curve was single exponential ($k = 0.02\ (\pm 0.05)\ min^{-1}$, data not shown), indicating that the reaction was first order in both O_2 and dithranol as in the acidic case.

To avoid complications due either to very slow equilibration of O_2 (pH 9.8) or reaction times (pH 6.3), the reaction order and rate constant for the dithranol reaction were measured by the method of initial rates using HPLC to monitor dithranol disappearance. This also allowed for the simplest direct comparison between the uncatalyzed and catalyzed reactions (Fig. 4*A*). Consistent with the expected second-order rate law, rate $= k$ $[O_2]$ [dithranol], the dependence of initial rate of dithranol disappearance on concentration was linear. From the slope of the line (k $[O_2]$) the second-order rate constants $k = 1.2\ (\pm 0.005) \times 10^{-4}$ and $3.6\ (\pm 0.005) \times 10^{-4}$ $\mu M^{-1}\ min^{-1}$ were computed at pH 6.3 and 9.8, respectively (Table 1).

Slower apparent rates of O_2 consumption relative to dithranol disappearance were observed for the same reactions. This is qualitatively consistent with a proposed mechanism where the $O_2^{\cdot-}$ product disproportionates to form O_2 and H_2O_2 (Scheme 2), thereby suppressing the apparent rate of O_2 consumption. The second-order rate constants measured via the HPLC method were therefore reported (Fig. 4*A* and Table 1).

Enzymatic Oxidation of Dithranol in Air—Dithranol disappearance was monitored via O_2 consumption under acidic and alkaline conditions identical to those used for determining the uncatalyzed second-order rate constants (see above) but in the presence of catalytic NMO (4 μM) (Fig. 4*A* and Table 2). Enzymatic rates were corrected for the background uncatalyzed reaction.

Under acidic conditions, the plot of initial rate *versus* [dithranol] fit well to the Michaelis-Menten model (Equation 4), yielding $k_{cat}/K_m = 0.050 \pm 0.01$ $\mu M^{-1}\ min^{-1}$ (pH 6.3). This is ~400-fold higher than the counterpart second-order rate constant measured under identical conditions but with no enzyme present.

Under basic conditions (pH 9.8), the initial rates fit to the Michaelis model with substrate inhibition. Fitting the data in Fig. 4*A* to Equation 5 yielded $k_{cat}/K_m = 0.58 \pm 0.04$ $\mu M^{-1}\ min^{-1}$, or about a 1600-fold increase relative to the uncatalyzed second-order rate constant. These values for k_{cat}/K_m are apparent because the O_2 concentration (air, 280 μM) was not saturat-

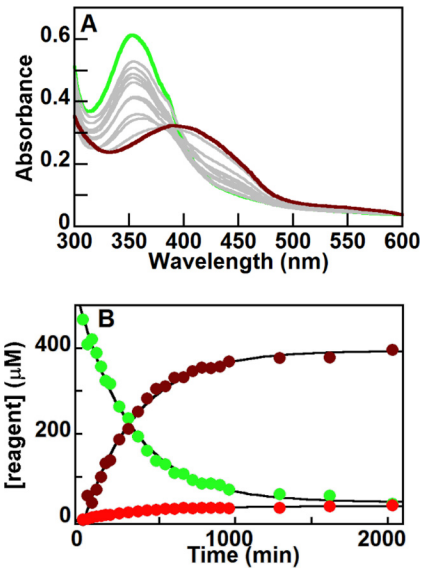

FIGURE 2. **Uncatalyzed dithranol oxidation under acidic conditions (pH 6.3) is very slow.** *A,* dithranol (*green*) converts to bisanthrone (*brown*) as its major product at pH 6.3 in air (100 μM starting dithranol, 20 °C, 0.1 M citrate/ME, *gray spectra,* measured at 30-min increments). The lack of an isosbestic point suggests the generation of more than one product. *B,* dithranol (500 μM) conversion monitored discontinuously over time by HPLC (*green circles*) clearly shows the appearance of the major product, bisanthrone (*brown circles*, 90% yield), as well as a small amount of dithranone (*red circles*, 10% yield) (0.1 M citrate/ME (pH 6.3), air). The disappearance of dithranol and appearance of bisanthrone occurred with first-order kinetics, $t_{1/2}$ = 240 min.

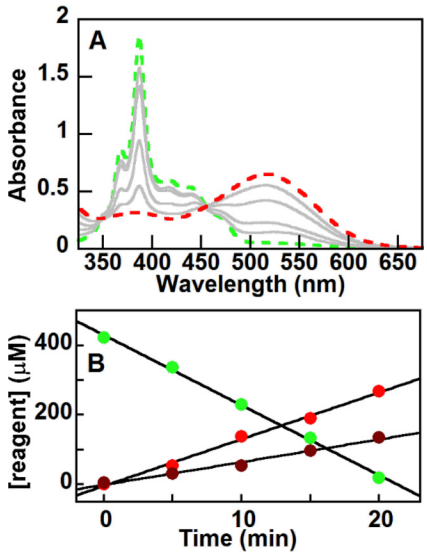

FIGURE 3. **Uncatalyzed oxidation of the dithranol anion is much more rapid under basic conditions (pH 9.8) and gives a different product distribution.** *A,* dithranol anion (*green dashes*) converts to approximately equal amounts of bisanthrone and dithranone (*red dashes*) over a period of 40 min at pH 9.8 in air (100 μM starting dithranol, 20 °C, 0.1 M CAPS/ME, *gray traces* measured at 5-min increments). *B,* dithranolate (500 μM) disappearance (*green circles, k* = 20 μM min^{-1}), monitored discontinuously by HPLC, was linear over time ($t_{1/2}$ = 13 min), converting into the alkaline forms of dithranone (*red circles, k* = 13 μM min^{-1}) and bisanthrone (*brown circles, k* = 6.7 μM min^{-1}).

TABLE 1

Kinetic constants and final product distributions for the non-enzymatic oxidation of dithranol

Reaction conditions are as follows: $[dithranol]_{initial}$ = 500 μM, air (280 μM), 20 °C, citrate/ME (pH 6.3) or CAPS/ME (pH 9.8) buffers. Reactions were gently stirred. Values for second-order rate constants, *k,* are obtained from the slopes of plots of the initial rate of dithranol disappearance *versus* [dithranol] (slope = $k[O_2]$). See Fig. 4*A*. Note that enzymatic rates were corrected for the nonenzymatic reactions.

pH	*k*	$t_{1/2}$	Bisanthrone	Dithranone
	$\mu M^{-1}\ min^{-1}$	*min*	%	%
6.3	1.2 (±0.005) × 10^{-4}	240[a]	90 ± 4	10 ± 4
9.8	3.6 (±0.005) × 10^{-4}	13[b]	40 ± 2	60 ± 2

[a] Reaction was first-order in dithranol; $k = 0.0028\ min^{-1}$ and $t_{1/2} = 0.693/k$.
[b] Reaction was pseudo-zero-order in dithranol under conditions where $[dithranol]_{initial} > [O_2]$ (air-saturated solvent). The value for $t_{1/2}$ is reported for $[dithranol]_{initial}$ = 500 μM, where k = 20 μM min^{-1} and $t_{1/2} = [dithranol]_{initial}/2k$.

ing; and because of the high K_m value for O_2, a saturating concentration of O_2 moreover could not be obtained (see below). However, they provide a functional measure of the reaction rate enhancement afforded by the presence of the enzyme in air. Finally, fitting Equation 5 to the data yielded K_i = 1100 ± 300 μM. This describes the dissociation of a molecule of dithranol (S) from the NMO-dithranol (*ES*) complex: $SES \leftrightarrows S + E$ (Table 2). The observed substrate inhibition implies that binding two molecules of dithranol to the enzyme suppresses further dithranol consumption. This suggests that, at high pH, bisanthrone production occurs outside of the enzyme.

pH Dependence of the Steady State Reaction—To understand the source of the pH dependence in the enzymatic reactions, apparent steady state kinetic parameters were measured over a range of pH values (5–11) using various concentrations of dithranol in air (20 °C). Data measured at pH values below the pK_a of dithranol (8.5) fit well to Equation 4. Above this pH, data required the use of the substrate inhibition model (Equation 5). Only the anionic form of dithranol appeared to bind *ES* to generate the inhibitory *SES* complex.

Plots of both $\log k_{cat}$ and $\log k_{cat}/K_m$[dithranol] increased markedly with pH (Fig. 4, *B* and *C*) and had slopes of ≈0.6, suggesting that a single deprotonation event controlled the conversion between a less reactive acidic and more reactive alkaline form. Fitting the data to Equation 7 yielded pK_a = 6.8 ± 0.05 (k_{cat}) and 6.7 ± 0.2 (k_{cat}/K_m[dithranol]). These values are more than 1.5 units smaller than the pK_a value measured for the substrate (8.5) in the same solvent system.

The pH dependence in Fig. 4 could be attributable to an active site base. Two possible candidates were identified by inspection of the NMO structure (Fig. 5). The enzyme is relatively small, containing a single open cavity between a series of α-helices and β-sheets where ethylene glycol from the crystallization solvent binds. His-49 points inward toward the cavity, whereas His-85 is on a stretch of helix that could conceivably rotate, positioning the side chain in the vicinity of the cavity. No other potential acid-base residues are present in the pocket. The pH-dependent kinetics of the H49A and H85A mutants were characterized as above (Fig. 4, *B* and *C*). The lack of any change in k_{cat} and k_{cat}/K_m[dithranol] over the entire pH range suggests that neither serves as an active site base residue and indeed neither is directly involved in the reaction. These conclusions are consistent with the finding that neither residue is well conserved among ABMs, although His-85 is conserved within the NMO-containing subfamily (see below).

Although not basic residues, two well conserved asparagines (Asn-18 and Asn-63) are within hydrogen bonding distance of a solvent molecule in the NMO active site (Fig. 5). Mutation of either (to non-polar alanine) was previously shown to strongly

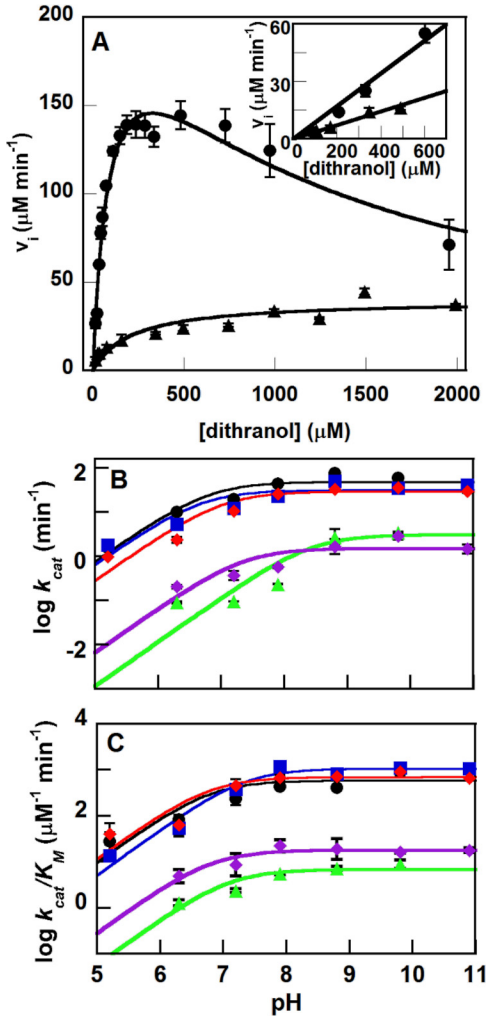

FIGURE 4. **Steady state NMO-catalyzed reaction is faster and exhibits substrate inhibition at higher pH.** *A*, initial rate of substrate (O_2) disappearance was monitored as a function of dithranol concentration at pH 6.3 (*circles*) and 9.8 (*triangles*) in the presence and absence (*inset*) of catalytic amounts of NMO (4 μM, 20 °C, air). Under moderately acidic conditions, the enzymatic reaction is slow and follows Michaelis-Menten kinetics (k_{cat} = 10 ± 0.3 min^{-1}, k_{cat}/K_m(dithranol) = 0.050 ± 0.01 μM^{-1} min^{-1}, and K_m = 220 ± 60 μM). Under basic conditions, the reaction is substantially faster and exhibits substrate inhibition: k_{cat} = 60 ± 6 min^{-1}, k_{cat}/K_m(dithranol) = 0.58 ± 0.04 μM^{-1} min^{-1}, and K_m = 100 ± 20 μM, K_i(dithranol) = 1100 ± 300 μM. *Inset*, second-order rate constants derived from the uncatalyzed reaction were k = 1.2 (±0.005) × 10^{-4} μM^{-1} min^{-1} (pH 6.3) and k = 3.6 (± 0.005) × 10^{-4} μM^{-1} min^{-1} (pH 9.8). Values of k_{cat} (*B*) and k_{cat}/K_m(dithranol) (*C*) were measured as a function of pH for NMO (*black circles*) and mutants as follows: H85A (*blue squares*), H49A (*red diamonds*), N63A (*purple diamonds*), and N18A (*green triangles*). The data for WT and the H mutants overlap (pK_a = 6.8 ± 0.05), indicating that neither histidine acts as an active site base was determined for all of the curves. The pK_a values for the N mutants were alkaline-shifted relative to WT: 8.6 ± 0.1 (k_{cat}) and 7.2 ± 0.05 (k_{cat}/K_m[dithranol]) (N18A); 7.6 ± 0.1 (k_{cat}) and 7.0 ± 0.2 (k_{cat}/K_m[dithranol]) (N63A).

impair the activity of the enzyme, although both mutant enzymes retain their structures (5). Although the data were near the limits of detection, the pK_a values observed for plots of both logk_{cat} and logk_{cat}/K_m[dithranol] for N18A and N63A NMO clearly shifted away from the WT values and toward the pK_a values for free dithranol: pK_a = 8.6 ± 0.1 (k_{cat}) and 7.2 ± 0.05 (k_{cat}/K_m[dithranol]) (N18A); pK_a = 7.6 ± 0.1 (k_{cat}) and 7.0 ± 0.2 (k_{cat}/K_m[dithranol]) (N63A). This suggests that both residues contributed to the pH dependence in the steady state reaction for WT NMO.

We hypothesized that Asn-18 or Asn-63 could suppress the pK_a value of dithranol by stabilizing its anionic form or acting as a conduit for released H^+. At pH 6.3, when the substrate is in its neutral form, both mutations strongly suppressed k_{cat} (120- and 50-fold for the N18A and N63A mutants, respectively). By contrast, the values for K_m were actually lower than for WT NMO. This suggests that reducing polarity at Asn-18/Asn-63 facilitates *ES* formation when the substrate is uncharged, but it impairs subsequent chemical steps.

The situation at pH 9.8, with dithranol in its anionic form, was the opposite. A relatively smaller (20-fold) effect was observed for k_{cat} for either mutant. However, K_m values for N18A and N63A were elevated 5- and 3-fold, respectively. For the anionic substrate, reduction in polarity in the active site strongly impairs *ES* formation with a proportionally smaller impact on chemistry (k_{cat}). These results suggest that polar residues Asn-18 and Asn-63 are most important for *ES* formation (K_m) when S is already in the anionic state and for catalysis (k_{cat}) when it is neutral/protonated, as it would primarily be at physiological pH. The k_{cat} effect could be due to either residue serving as a proton conduit.

Dependence of Substrate Affinity on pH—To further probe the effects of pH, the affinity of WT NMO and the N18A/N63A mutants for dithranol was measured. Under acidic conditions (pH 6.3), K_d = 0.73 ± 0.004 μM. This decreased roughly 10-fold to 0.069 ± 0.03 μM at pH 9.8, indicating that NMO binds the substrate anion with greater affinity. For the N63A mutant protein, K_d = 0.69 ± 0.02 μM (pH 6.3) and 0.20 ± 0.01 μM (pH 9.8). For the N18A mutant, K_d = 0.33 ± 0.009 μM (pH 6.3) and 1.4 ± 0.2 μM (pH 9.8). These results showed that N18A and N63A have approximately the same affinity for neutral dithranol as the WT NMO (pH 6.3). However, both Asn-18/Asn-63 are important for the pronounced NMO/substrate affinity observed specifically at high pH.

Dependence of the Steady State Enzymatic Reaction on O_2 Concentration—Initial rates of the reaction between the NMO-substrate complex and O_2 were measured in the presence of dithranol (250 μM) with various concentrations of O_2 using the O_2 consumption assay (Fig. 6*A* and Table 2). Under acidic conditions (pH 6.3), fitting Equation 4 to the data yielded k_{cat} = 13 (±0.9) min^{-1}, $K_m(O_2)$ = 430 μM, and $k_{cat}/K_m(O_2)$ = 0.030 ± 0.003. Above the observed enzymatic pK_a (pH 9.8), the rate of the reaction increased substantially. Although a saturating [O_2] could not be reached, the apparent K_m from fitting the data to Equation 6 was 410 μM. This fit also predicted a Hill coefficient of 1.8, indicating positive cooperativity. This suggests that the O_2 reaction at one of the two subunits of NMO potentiates a reaction at the second by an unknown mechanism.

The measured $k_{cat}/K_m(O_2)$ = 0.26(± 0.01) min^{-1} was 730-fold greater than the second-order rate constant for the reaction of dithranol and O_2 determined under identical conditions but with no enzyme present (Fig. 4*A* and Table 1). The $k_{cat}/K_m(O_2)$ was furthermore 2-fold less than the k_{cat}/K_m(dithranol) measured in air. The k_{cat}/K_m values can be regarded as a second-order rate constant encompassing all microscopic chemical steps involving a given substrate up to and including the one that is rate-limiting. Because $k_{cat}/K_m(O_2) < k_{cat}/K_m$(dithranol),

TABLE 2

Kinetic constants for the steady state enzymatic oxidation of dithranol

Reaction conditions are as follows: varied concentrations of dithranol were used in air (sub-saturating, 280 μM O_2), 4 μM NMO, 20 °C, citrate/ME (pH 6.3) or CAPS/ME (pH 9.8) buffers. The measured value for k_{cat} is apparent because a sub-saturating amount of O_2 was used.

pH	k_{cat}	K_m (dithranol)	k_{cat}/K_m(dithranol)	K_m (O_2)[a]	$k_{cat}/K_m(O_2)$[a]	K_I	Bisanthrone[b]	Dithranone[b]
	min^{-1}	μM	$\mu M^{-1}\ min^{-1}$	μM	$\mu M^{-1}\ min^{-1}$	μM	%	%
6.3	10 ± 0.3 13 ± 0.9[a]	220 ± 60	0.050 ± 0.01	430	0.030 ± 0.003	N/A	50 ± 3	50 ± 3
9.8	60 ± 6 110 ± 6[a]	100 ± 20	0.58 ± 0.04	410	0.26 ± 0.01	1100 ± 300[a]	10 ± 2	90 ± 2

[a] Reaction conditions are as follows: varied concentrations of O_2 were used in constant dithranol (250–500 μM), 4 μM NMO, 20 °C, citrate/ME (pH 6.3), or CAPS/ME (pH 9.8) buffers.

[b] Reaction conditions are as follows: 500 μM dithranol, air (280 μM), 1 mM NMO, 20 °C, 30 min incubation, citrate/ME (pH 6.3) or 500 μM dithranol, air (280 μM O_2), 50 μM NMO, 10 min incubation. CAPS/ME (pH 9.8).

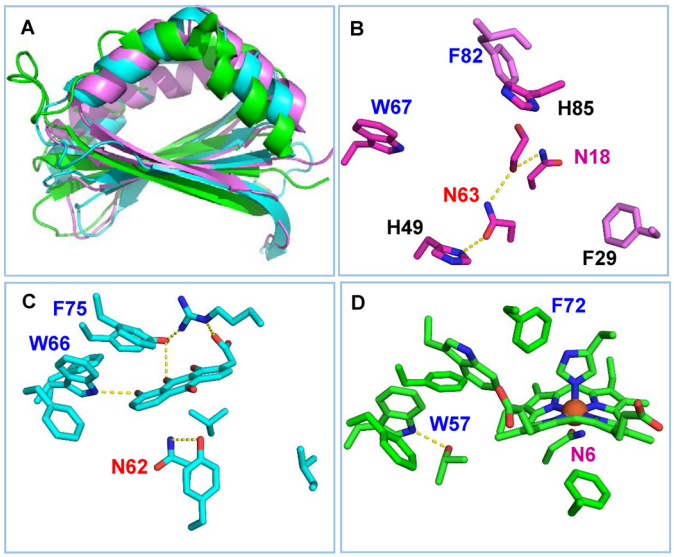

FIGURE 5. **Domain and active site structures of NMO (*violet*), ActVA-Orf6 (*cyan*), and IsdI (*green*) (Protein Data Bank codes 3KG0, 1N5T, and 3LGN).** *A*, overlay of substrate-binding domain of all three proteins, rendered as schematics. *B–D*, active site residues conserved within each subfamily are shown, with the protein in the same orientation as in *A*. Interactions that could be hydrogen bonds (distances ≤3.5 Å) are indicated with *dashed lines*. Conserved residues are shown and their labels color-coded. *Blue* labels indicate conservation among all three subfamilies; *red* indicates NMO and ActVA-Orf6; *purple* indicates NMO and IsdI; *black* indicates conserved only within the subfamily shown. Note that His-85 (NMO numbering used) is conserved within the NMO subfamily but not the ActVA-Orf6 subfamily. His-49 is highly but not strictly conserved, even within the NMO cluster, but it was examined nonetheless because of its key position. Asn-63 is conserved in both NMO and ActVA-Orf6 subfamilies. Additionally, the functionally important asparagine in the IsdG/Is (Asn-6) is conserved in the NMO subfamily (as Asn-18) but not among ActVA-Orf6 and its close relatives (8). Notably, no positively charged or acid-base residues are conserved between the NMO and ActVA-Orf6 clusters, arguing against their involvement in a common reaction mechanism. The iron-ligating histidine residue that is strictly conserved in IsdG/Is is not conserved in either the NMO or ActVA-Orf6 clusters.

it was concluded that a step involving O_2 must limit the overall rate of the NMO-catalyzed reaction.

Transient Kinetics of the Reaction between the NMO-Dithranol Complex and O_2—Stopped-flow experiments were carried out by mixing the anaerobic enzyme-substrate complex in one syringe with O_2-equilibrated solutions in the other (pH 9.8). NMO was highly concentrated and present in excess of dithranol to ensure that substrate would be enzyme-bound. The reaction occurred in two readily identifiable phases, each of which fit well to a single exponential curve (Fig. 6, *B* and *C*). Under air, the initial phase was complete within ≤5 s, whereas the second slower phase took on the order of 300 s (Fig. 6*B*). Carrying out

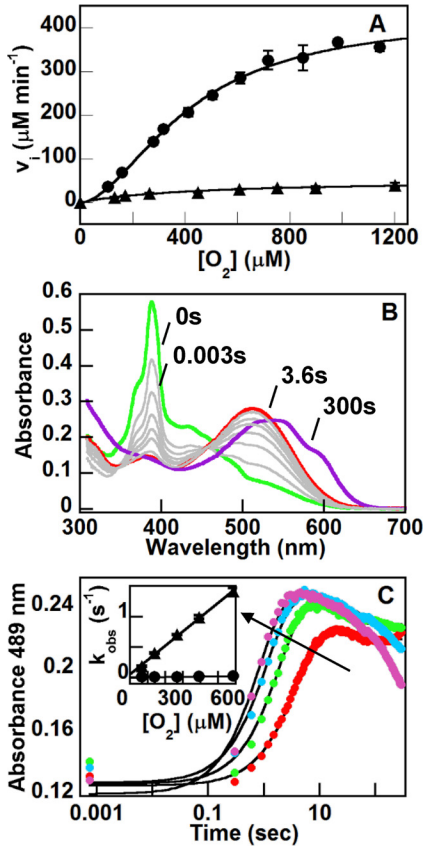

FIGURE 6. **NMO-catalyzed steady state and single turnover reactions of dithranol and O_2 show that an O_2-dependent step limits the overall reaction rate.** *A*, initial rate of O_2 disappearance was monitored as a function of O_2 concentration at pH 6.3 (*triangles*) and 9.8 (*circles*). Fitting the data at pH 6.3 (500 μM dithranol, citrate/ME, 20 °C) to the Michaelis-Menten model (Equation 4) yielded the following: $k_{cat} = 13 \pm 0.9\ min^{-1}$, $K_m(O_2) = 430$ mM, and $k_{cat}/K_m(O_2) = 0.03 \pm 0.003\ \mu M^{-1}\ min^{-1}$. At pH 9.8 (250 μM dithranol, CAPS/ME, 20 °C), a model including positive cooperativity yielded $k_{cat} = 110 \pm 6\ min^{-1}$, $k_{cat}/K_m(O_2) = 0.26 \pm 0.01\ \mu M^{-1}\ min^{-1}$, $K_m = 410\ \mu$M, and $n = 1.8$ (Hill coefficient). *B*, reaction between the anaerobic 30 μM NMO-dithranolate complex and 608 μM O_2 (CAPS/ME (pH 9.8), 20 °C) was monitored over time following rapid mixing. The initial conversion of the starting complex (*green spectrum*) to a species with a spectrum resembling the alkaline form of dithranone (*red*) was complete within ~3.6 s. This species subsequently converted very slowly to the final observed photoproduct (*purple*) within ~300 s. The *gray spectra* were measured at 0.3-s increments. *C*, single wavelength traces (389 nm and 66, 137, 262, 392, and 608 μM O_2) plotted *versus* time illustrate the two kinetic phases shown in *A*. Data were fit to the sum of two exponentials to obtain values of $k_{obs}(1)$ and $k_{obs}(2)$, and the *arrow* shows the direction of increasing O_2 concentrations. *Inset*, values for k_{obs} were plotted *versus* O_2 concentration. The initial kinetic phase exhibited a strong linear dependence on [O_2], yielding the second-order rate constant $k_1 = 0.14 \pm 0.005\ \mu M^{-1}\ min^{-1}$. The second phase, ascribed to the photodegradation of the product, was far slower and independent of O_2 concentration.

the reactions with various concentrations of O_2 showed that the first phase was clearly O_2-dependent with a second-order rate constant $k = 0.14 \pm 0.005\ \mu M^{-1}\ min^{-1}$ (Fig. 6*C*, *inset*). This number is similar to the measured value for $k_{cat}/K_m(O_2)$ ($0.26 \pm 0.01\ \mu M^{-1}\ min^{-1}$), consistent with the expectation that both constants are kinetically limited by the same step of the reaction. The second phase was independent of the concentration of O_2. Comparison of the data to a no-enzyme control indicated that the slow phase is due to conversion of dithranone to a photoproduct on exposure to the intense white light of the xenon lamp and that the rate of this phase is directly dependent on the intensity of incident light on the reaction mixture. This is consistent with the known photoreactivity of anthracenone compounds (29).

Radical Pair Formation and Recombination—Prior work has suggested that bisanthrone forms via the initial generation of a dithranyl radical/$O_2^{\cdot-}$ pair that does not undergo recombination (29, 30–32). Consistent with that expectation, when dithranol, O_2, and CMH were incubated at pH 6.3 (major product: bisanthrone), the continuous slow conversion of CMH to CM$^{\cdot}$ was observed by EPR for ≥120 min (data not shown). Because the half-life of CM$^{\cdot}$ under these conditions is on the order of 6 h (31), experiments were confined to the initial phase of the dithranol reaction. Notably, in control experiments carried out in the presence of 2500 units/ml SOD (see below), no CM$^{\cdot}$ was observed by EPR. This confirmed that CM$^{\cdot}$ was generated by reaction with $O_2^{\cdot-}$ rather than dithranyl radical.

A related mechanism for dithranone formation can be proposed in which a dithranyl/$O_2^{\cdot-}$ pair forms ($\uparrow$)($\uparrow$), undergoes a spin transition ($\uparrow$)($\downarrow$), and subsequently recombines ($\uparrow\downarrow$) (Schemes 1 and 2). Breakdown of the resulting (hydro)peroxyadduct by heterolytic cleavage of the O–O bond yields dithranone and H_2O. If this mechanism is correct, superoxide scavengers could in principle disrupt the dithranyl/$O_2^{\cdot-}$ pair, leading to the release of free dithranyl. Two neutral dithranyl radicals could then couple to form bisanthrone, biasing the product ratio (bisanthrone/dithranone) toward bisanthrone.

To test this hypothesis, experiments were carried out using CMH and SOD as $O_2^{\cdot-}$-scavenging reagents at pH 9.8, where dithranone was the observed major product for both the catalyzed and uncatalyzed reactions (Tables 1 and 2). We expected that either SOD or CMH could compete with dithranyl/$O_2^{\cdot-}$ recombination in free solution. However, because of its size, SOD should have no effect on reactions occurring inside the NMO-active site. The products of the uncatalyzed reaction (500 μM dithranol, air) at pH 9.8 in the presence of increasing equivalents of CMH (with respect to dithranol) were analyzed. The dithranone/bisanthrone ratio decreased roughly linearly from 60:40 to 25:75 as CMH eq increased from 0 to 10 (−3.2% per CMH, Fig. 7*A*). SOD had an analogous influence; a concentration of 1250 units/ml gave results comparable with 10 eq CMH. The SOD effect saturated near 5000 units/ml, with ≥80% bisanthrone. Notably, the presence of $O_2^{\cdot-}$-trapping agents did not appreciably extend the incubation time needed to deplete the entire initial concentration of dithranol. This observation is consistent with a slow dithranol/O_2 reaction to form dithranyl/$O_2^{\cdot-}$ with faster subsequent steps.

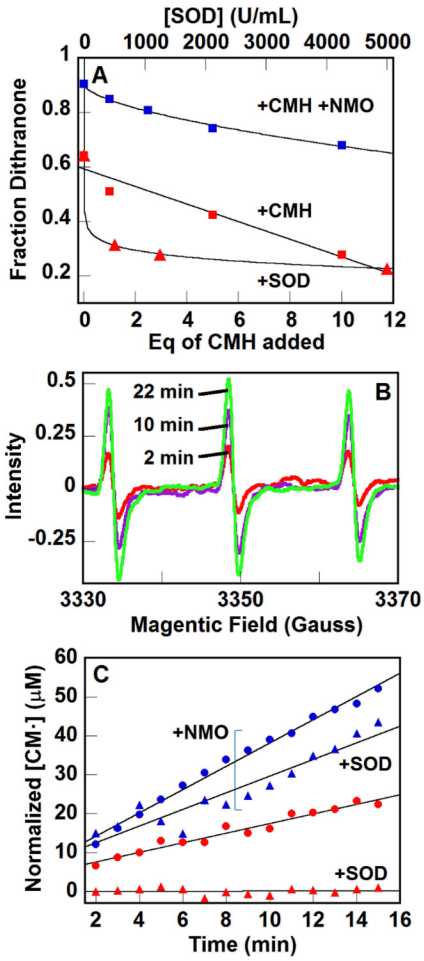

FIGURE 7. **Superoxide is generated during the catalyzed and uncatalyzed reactions and is an intermediate to the monooxygenase product, dithranone.** *A,* products of the uncatalyzed reaction at pH 9.8 (CAPS/ME, 500 μM dithranol, 22 °C) were analyzed by HPLC after the reactions had gone to completion in the presence of increasing concentrations of CMH (*red squares*) or SOD (*red triangles*). The dithranone fraction is plotted, and the remainder was bisanthrone. The products of the catalyzed reaction (+50 μM NMO) were analyzed after the reaction had gone to completion in the presence of increasing concentrations of CMH (*blue squares*). The enzymatic reaction (90% dithranone product) was largely unaffected by even the highest concentration of SOD; hence the data are not shown. *Lines* or extrapolated *smooth curves* illustrate the trends in the data. *B,* reaction of 200 μM dithranol (used as limiting reagent due to lack of sample equilibration with air), air, 280 μM O_2, 5 μM NMO, and 10 eq CMH (2 mM) to yield CM$^{\cdot}$ was monitored over time by EPR (pH 9.8, CAPS/ME, 22 °C). Data were measured every minute until the spectrum stopped growing in intensity. Spectra measured at selected time points with their *y* axis normalized to TEMPO standard concentrations are shown. *C,* time-resolved spectra were measured as in *B* in the presence (*blue symbols*) and absence (*red symbols*) of 5 μM NMO. *Circles* represent reactions carried in the presence of CMH as the means for superoxide detection, and *triangles* are for reactions carried out with both CMH and added SOD (2500 units/ml). The catalyzed reaction generates CM$^{\cdot}$ more quickly than the uncatalyzed. Only the uncatalyzed reaction is significantly affected by competition with SOD, suggesting that $O_2^{\cdot-}$ is protected from SOD inside the NMO active site.

Under the same conditions but with added NMO (50 μM), 5000 units/ml SOD (a saturating amount in the uncatalyzed reaction, Fig. 7*A*) had only a modest effect on the NMO-catalyzed reaction, lowering the dithranone/bisanthrone ratio from 90:10 to ~80:20. The relative insensitivity of the ratio to SOD suggested that either superoxide was not involved in the NMO-catalyzed reaction or that dithranone is primarily generated from a dithranyl/$O_2^{\cdot-}$ pair that is sterically protected inside

NMO. By contrast, CMH suppressed the dithranone/bisanthrone ratio as in the uncatalyzed case, although to a lesser extent (10 eq CMH led to 70:30 dithranone/bisanthrone). Truncation of the effect may due to the limited affinity of CMH for NMO, competitive effects between the substrate and CMH, or both.

The production of $O_2^{\cdot-}$ during the dithranol oxidation reaction was subsequently monitored over time via EPR at pH 9.8 (Fig. 7*B*). Superoxide trapping (detected via CM$^{\cdot}$) was linear with time (1.2 μM min^{-1}) over the initial portion of the reaction. In the presence of 2500 units/ml SOD, the same reaction yielded CM$^{\cdot}$ at just above the baseline level although the dithranone/bisanthrone ratio was 25:75. This suggested that $O_2^{\cdot-}$ was preferentially scavenged by SOD. In the presence of 5 μM NMO, more rapid CM$^{\cdot}$ production was observed during the initial phase of the reaction (3.0 μM min^{-1}). Moreover, in contrast to the uncatalyzed reaction, the rate of CM$^{\cdot}$ production was modestly affected by 2500 units/ml SOD. These results are consistent with the conclusion that $O_2^{\cdot-}$ generated inside NMO is accessible to CMH but not SOD.

Analysis of Sequence and Structure—The ABM family (45,000 known sequences) is large and contains biochemically characterized oxidases (QuMo (7)) and oxygenases (ActVA-Orf6 (8), NMO, IsdGs (20)), as well as a large number of undescribed proteins that have no documented reactivity. Network analysis was carried out to divide the family into functionally cohesive subfamilies (Fig. 8). At a stringency sufficient to separate the well characterized IsdGs as a discrete cluster (e^{-15}), at least 20 distinct subfamilies are observed. Notably, although both catalyze monooxygenase reactions on polyketide antibiotic substrates, ActVA-Orf6 and NMO partition to separate subfamilies. Residues conserved within and between clusters are shown in Fig. 5.

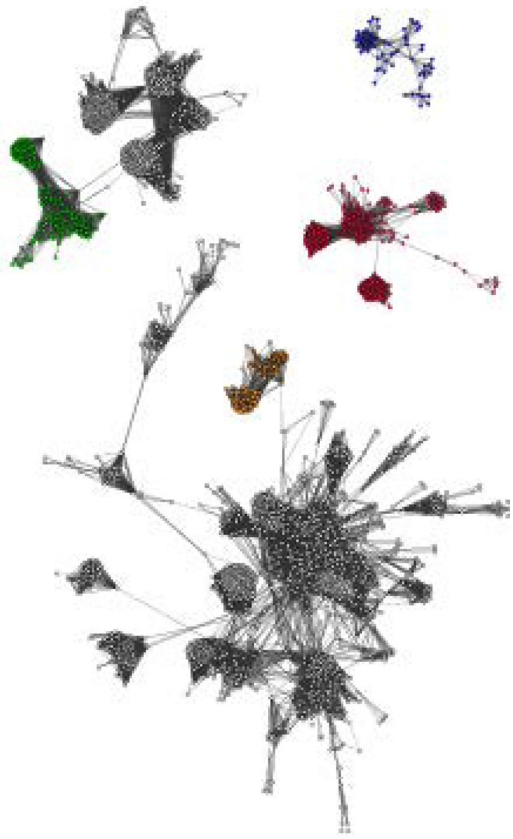

FIGURE 8. **Sequence analysis illustrates the diversity of the ABMs and the monooxygenase subfamilies within it.** Network analysis (stringency $e = 10^{-15}$) divided the >45,000 unique sequences of the family into at least 24 subfamilies, of which the NMO subfamily and its nearest neighbors are depicted here as clusters of dots (each *dot* contains closely related individual sequences). Partitioning of the functionally distinct heme-degrading IsdGs (*green dots*) into a discrete cluster was used to guide for the appropriate stringency, which led to the division of NMO and its neighbors (*blue dots*) into a separate family from ActVA-Orf6 (another characterized monooxygenase in an antibiotic biosynthesis pathway) and its closest homologs. *QuMo*, a quinol monooxygenase, and its closest relatives are shown as *orange dots*.

Discussion

ABMs catalyze oxygenation reactions using no metal or organic cofactors, depending instead on the protein environment alone for catalysis. The highly activated nature of many ABM substrates has led to the suggestion that they act *in lieu* of cofactors, and a specific but largely untested analogy to flavoprotein chemistry has been drawn (2). The environment inside flavin-dependent oxidases and oxygenases indeed has an extraordinary influence over the cofactor, enhancing the rate of its oxidation by 10^4–10^6-fold over the reaction in free solution (10). Here, using the ABM from the nogalamycin biosynthetic pathway (NMO), we examined whether flavoprotein-like catalytic strategies (Scheme 1) were at work, comparing the uncatalyzed and catalyzed reactions.

At least three well described features of the flavin/O_2 reaction were considered in the context of NMO. First, both the flavin cofactor and the substrate that it oxygenates react faster in their anionic deprotonated forms (33, 34). Although removal of the substrate proton is often base-catalyzed in flavoproteins (35), the relatively acidic flavin (pK_a of flavin-N_1H $\approx$ pH 7) is stabilized in its anionic form by a strategically positioned positive charge or a hydrogen bonding partner (36). In keeping with this model, the pH-rate profiles for the NMO reaction (k_{cat} and k_{cat}/K_m) showed that the alkaline enzyme-substrate complex reacts more rapidly than the acidic form (Fig. 4) by nearly 2 orders of magnitude with a pK_a of 6.8 (dithranol pK_a = 8.5). The structure and sequence of NMOs were examined for evidence of base catalysis, identifying well (His-85) and poorly (His-49) conserved potential bases in the open NMO cavity (Fig. 5). However, when either was mutated to alanine, there was no observable effect on either the magnitude or the pH dependence of the steady state constants (Fig. 4). Given the absence of any other plausible residue, this suggested that NMO function does not depend on general base catalysis.

This stands in sharp contrast to HOD, the recently characterized cofactor-free dioxygenase, which undergoes a 5500-fold diminution in k_{cat} when its active site base is eliminated (23). Given the relative acidity of the NMO substrate, we considered the possibility that the protein may exert a more subtle effect. Specifically, Asn-63 and Asn-18 are strictly conserved within the NMO sequence cluster (Fig. 8) and are obvious candidates for hydrogen bonding to the substrate (Fig. 5). Consistent with prior observations (5), N63A and N18A mutant proteins exhibited activity that was strongly suppressed over the entire pH range examined. However, both still bound the neutral/proto-

nated substrate with affinity similar to that of the WT enzyme (pH 6.3). At pH values greater than the pK_a of the substrate, the binding affinity diminished by 3- and 20-fold, respectively, for the N63A and N18A mutants. Parallel effects were observed for K_m. This suggested that an interaction with both residues helps to selectively stabilize the anionic form of the substrate and might be partly responsible for lowering its pK_a. Suppressed values for k_{cat} further suggested that these residues play an additional catalytic role.

A second defining feature of flavoprotein/O_2 catalysis is the formation of a semiquinone/$O_2^{\cdot-}$ radical pair in a rate-limiting step (Scheme 1*A*). The barrier to this important step is lowered by the enzyme, sometimes via a well positioned positive charge that stabilizes superoxide and thereby minimizes the reorganization energy following electron transfer (37–40).

An analogous substrate radical/$O_2^{\cdot-}$ pair can be proposed at the NMO-active site (Scheme 1*B*); however, such an intermediate is not obligate. As an alternative, the protein could stabilize the substrate or an intermediate in a radical doublet ($\downarrow$) state, which could react directly with triplet O_2 ($\uparrow\uparrow$) to form a doublet substrate/O_2 adduct ($\downarrow$). Such a reaction would not violate the spin rule and hence could occur rapidly. In fact, Trp-66, one of a handful of strictly conserved residues in the heme-degrading IsdG family (Fig. 5), has been shown to deform the normally planar heme inside these enzymes. Such ruffling induces unpaired electron density in the *meso*-carbons of the tetrapyrrole (20, 41, 42), thereby facilitating the direct reactions between O_2 and heme (43, 44). A mechanism involving induction of radical character in the substrate has also been proposed for the oxidation of urate by the cofactor-independent urate oxidase (45, 46). Catalysis could alternatively involve formation of a triplet state di-radical adduct between the singlet substrate and triplet O_2. Recent experimental and computational evidence suggested that the anion of the substrate for HOD reacts directly with O_2 to form such an intermediate in a step that limits the overall reaction rate (22).

In investigating the O_2 reactivity of NMO, we found that, consistent with the flavoenzyme paradigm, the reaction between dithranol and O_2 occurs as a slow step (Fig. 6). We then tested the hypothesis that a dithranyl/$O_2^{\cdot-}$ radical pair is the key catalytic intermediate that forms in the slow step, finding three kinds of evidence in support. First, a stable substrate radical inside the anaerobic NMO-substrate complex was not observed by EPR, arguing against a urate-oxidase-like activation of the substrate (data not shown). Second, using enzymatic (SOD) and small molecule (CMH) superoxide-trapping agents (Fig. 7*A*), the intermediacy of superoxide was confirmed for the uncatalyzed dithranone-forming pathway. Both were able to reverse the 60:40 ratio of dithranone/bisanthrone (pH 9.8) toward near-complete formation of bisanthrone, presumably due to the scavenging of $O_2^{\cdot-}$ away from a dithranyl/$O_2^{\cdot-}$ pair. A similar although smaller effect on the product ratio was observed for the NMO-catalyzed reaction carried out in the presence of CMH (Fig. 7*A*) but not SOD, suggesting that $O_2^{\cdot-}$ generated inside NMO could be quenched by reaction with the small molecule CMH. Third, the amount of CM$^{\bullet}$ formed by the dithranol/O_2 reaction, monitored by EPR, diminished in the presence of SOD for the uncatalyzed reaction, suggesting that CMH and SOD could compete for $O_2^{\cdot-}$. However, SOD had no effect on CMH/$O_2^{\cdot-}$ trapping in the presence of NMO (Fig. 7*C*). Collectively, these experiments point toward a dithranyl/$O_2^{\cdot-}$ pair as a key intermediate on either the catalyzed/uncatalyzed pathway leading to the oxygenated product. Distinct from many flavoenzymes, there is no stable positive charge in the active site, although the amide side chains of Asn-63 and/or Asn-18 have charged resonance forms. Either of these residues could play a role in accelerating the formation of the radical pair.

A third and final role for the enzyme in flavin-dependent oxidases/oxygenases is in steering highly reactive intermediates toward a single set of products. This role asserts itself around at least two major decision points in the mechanisms of flavoenzymes (10). First, the initially formed flavin semiquinone/$O_2^{\cdot-}$ radical pair is in the triplet state (two unpaired electron spins) (9). The radicals in the pair can drift apart, generating the semiquinone and $O_2^{\cdot-}$ as the ultimate products. This is the observed outcome for flavin-dependent electron transferases as well as cryptochromes, light-receptor flavoprotein oxidases that use the resulting superoxide as a diffusible signaling agent (47–49). It is also a principal reaction pathway for free flavin in solution, where autocatalytic reactions between the flavin semiquinone and O_2 or $O_2^{\cdot-}$ compete with the enzymatically driven recombination (10). Alternatively, the two electron spins can pair and the radicals rejoin, forming the flavin-C4a-OO^- adduct. With the addition of a proton, this adduct becomes the central C4a-OOH reactive species of flavin monooxygenases and some oxidases. The pendant peroxy group can either depart from the flavin as H_2O_2 (oxidases) or the O–O bond can cleave heterolytically as the terminal oxygen is incorporated into a substrate (oxygenases). In the latter case, the enzyme selects the appropriate substrate and tunes the oxidant toward either nucleophilic or electrophilic attack.

Because there is no adjacent imine nitrogen on dithranol to act as an electron sink, the analogous dithranyl-OOH adduct would appear to obligately follow the pathway in Schemes 1 and 2. This path predicts movement of the C10 hydride to the C10 oxygen, heterolytic O–O cleavage, and release of water. The critical steps controlling the outcome of the reaction therefore appear to be those that mediate the propensity of the radical pair to recombine or part ways. For the uncatalyzed reaction (Table 1 and Figs. 2 and 3), pH is clearly a key factor in this decision. First, the O_2-dependent disappearance of dithranol accelerates dramatically with pH, with reaction time scales moving from hours to minutes. The acceleration is attributable to the faster formation of a dithranyl/$O_2^{\cdot-}$ pair as the pH increases. Second, the product distribution becomes more markedly biased toward dithranone, the oxygenase product, with increasing pH.

The NMO-catalyzed reaction exhibited the same pH-dependent trends in rate and product distribution, but to an even more marked extent. Together, these results suggested that the enzyme has two major functions. First, it catalyzes the formation of the radical pair, in a reaction that is faster when the substrate is deprotonated and where Asn-63 and/or Asn-18 may serve key roles. Second, it directs the radical pair away from the path of mutual dissociation and toward that of the

recombination product, dithranone. The fact that bisanthrone is still a product of the enzymatic reaction at pH 6.3 suggests that these two functions are not strictly coupled; the radical pair can form under catalyzed conditions and then leave the active site without recombining, leading to bisanthrone on a time scale of minutes rather than hours (uncatalyzed reaction).

How NMO selectively enforces the recombination at higher pH values is not clear. However, recombination, whether in the catalyzed or uncatalyzed process, appears to be the preferred route as the pH increases. Under these conditions, the substrate radical is neutral, rather than a protonated radical cation (Scheme 2). The possible connection between the protonation state of the dithranyl and its subsequent reactivity will be examined in future work.

The paradigms for enforcing "cofactorless O_2 catalysis" are remarkably diverse. Although urate oxidase stabilizes a substrate radical and HOD a triplet substrate/O_2 diradical adduct, NMO follows a third route, where the enzyme clearly plays a major role in both forming and directing the reactivity of a dithranyl/O_2^- pair. How does NMO lower the barrier ($\Delta G^{\ddagger}$)? The uncatalyzed oxygenation of the substrate anion (pH 9.8) is orders of magnitude slower than the NMO-catalyzed process, illustrating that substrate deprotonation is not the primary function of the enzyme. At the same time, catalysis must be due to more than desolvation or restriction of substrate translational and rotational motions. Illustrating the point, the N63A and N18A mutants, which have fully intact structures and bind the substrate with reasonable affinity, have strongly impaired activity.

Instead, the principal role in catalysis appears to come ultimately from the ability of NMO to facilitate formation of a dithranyl/O_2^- pair. According to classic transition state theory (50), if the non-enzymatic and enzyme-catalyzed reactions share a similar transition state (as appears likely here), then dissociation constants for each ($K_N^{\ddagger}$ and $K_E^{\ddagger}$) can be written, where *E* is a spectator in the uncatalyzed case. The thermodynamic cycle can then be closed with the addition of two constants, K_S and K_T, as shown in Scheme 3. In Scheme 3, K_T is the dissociation constant for the substrate transition state from $ES^{\ddagger}$. In the simple transition state theory model, the enzyme accelerates the rate of reaction by stabilizing $ES^{\ddagger}$ or, in other words, by lowering K_T. Relating these constants to rates, if k_E describes the rate-limiting chemical transformation of *ES* to *EP* (equivalent to k_{cat} in the Michaelis model) and k_N describes the same step in the uncatalyzed case, then we get Equation 1.

$$k_E/k_N = K_E^{\ddagger}/K_N^{\ddagger} = K_S/K_T \qquad \text{(Eq. 1)}$$

Inserting values measured under identical conditions for the nonenzymatic and NMO-catalyzed reactions ($k_E = 60\ min^{-1}$, $k_N = 0.02\ min^{-1}$, $K_S = 0.069\ \mu M$ (pH 9.8), air, 20 °C, 30 μM S or *ES* complex) yields $K_T = 0.023$ nM. The associated extent of transition state stabilization for K_T relative to K_S is, therefore, 19 kJ mol^{-1}. In terms of magnitude, this is on the order of 2–3 hydrogen bonding interactions.

A more detailed investigation of the energy landscape promoting both the formation and recombination of the radical pair in NMO may allow us to understand the nature of the transition state and the enzyme structural features that promote its formation. These investigations may serve to support the development of catalysts that use O_2 from the air and obviate the need for fragile, expensive, and nonrenewable cofactors.

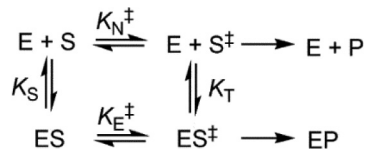

SCHEME 3

Experimental Procedures

Expression and Purification of NMO—The gene encoding the N-terminally His_6-tagged NMO (pBad vector) was received as a kind gift from the Schneider laboratory, University of Turku, Finland (5, 6). The NMO was expressed and purified as described previously (6). The purified enzyme mass was verified by electrospray ionization mass spectrometry.

Generation of Site-directed Mutants—Site directed mutagenesis was carried out using a QuikChange lightning kit (Agilent Technologies), the pBAD/His-NMO construct. Cultures of *E. coli* Top10 cells containing the mutant plasmids were grown, and the proteins were expressed and purified using the same protocol as for WT NMO.

Dithranol Stocks and Reaction Media—Dithranol (1,8-dihydroxy-9,10-dihydroanthracen-9-one, MP Biomedicals) was used as a surrogate for the natural NMO substrate (Scheme 1) (5, 6). Stocks (10 mM) were prepared in N_2-equilibrated dimethyl sulfoxide (DMSO) in septum-sealed vials inside an anaerobic chamber (Coy) immediately prior to use. The DMSO stock was diluted into reaction media consisting of 1:2 (v/v) buffer/ME. The organic ME component was essential for solubilizing the substrate and product. All buffers were prepared at 0.1 M, supplemented with 0.3 M NaCl, and adjusted to the desired pH as follows: citrate (pH 4.2–6.3), BES (pH 6.6–7.6), Tricine (pH 7.4–8.4), CHES (pH 8.3–9.3), and CAPS (pH 9.8–10.8).

NMO/Substrate Binding Monitored by Fluorimetric Quenching—NMO/dithranol binding was monitored via quenching of the intrinsic fluorescence of the protein on forming the enzyme-substrate (*ES*) complex. Dithranol (1.25 mM) was added via air-tight syringe (Hamilton) to a septum-sealed N_2-purged cuvette containing 6.5 μM NMO (pH 6.3 or 9.8) and allowed to equilibrate. 1,4-Dithiothreitol (DTT) (1 mM) was added to both the dithranol titrant solution and protein solution to remove residual O_2 and stabilize thiols Fluorescence measurements were made using a Cary50i fluorometer at room temperature with an excitation wavelength of 295 nm (tryptophan) and emission scanned from 300 to 400 nm (emission $\lambda_{max} = 328$ nm). The percentage of quenched fluorescence intensity was plotted against [substrate] and fit to Equation 2 to obtain K_D,

$$\Delta F_{obs} = \frac{\Delta F_{max}}{2E_t}\left(L_0 + E_t + K_D - \sqrt{(L_0 + E_t + K_d)^2 - 4E_t \cdot L_0}\right) \qquad \text{(Eq. 2)}$$

L_0, E_t, K_D, and ΔF_{max} are the ligand concentrations, total protein (subunit) concentration, the equilibrium dissociation constant, and the maximum % fluorescence that was quenched.

pH Titration of Dithranol—Aliquots of dithranol (100 μM) (Tris-ME (pH 5.0), 20 °C) were titrated with 1 N NaOH and their pH (Corning 430 pH electrode) and ultraviolet-visible spectra were measured (Cary60i spectrometer). Absorbance values at spectral maxima were plotted *versus* pH and fit as shown in Equation 3,

$$y = (B \times 10^{-pH} + A \times 10^{-pK_a})/(10^{-pH} + 10^{-pK_a}) \quad \text{(Eq. 3)}$$

where A and B are the highest and lowest absorbance values, respectively.

Analysis of Reactants and Products by HPLC—Dithranol and its quinonoid oxidation product dithranone (Sigma) were dissolved (500 μM) in 1:1 Tris-ME/tetrahydrofuran in an anaerobic chamber. The dimeric product, bisanthrone, was prepared by exposing 500 μM dithranol under acidic conditions to atmospheric O_2 (>60 min, 20 °C, Tris-ME (pH 6.3)) (51, 52). An Agilent 1100 series HPLC instrument with diode array UV-visible detection (300–700 nm) was used as follows: flow rate of 1.5 ml/min, 50 °C, 20-μl injection volume, Phenomenex Luna C18 3μ column, 150 × 4.6 mm. The solvents were 99.9% H_2O, 0.1% TFA (solvent A) and 99.9% acetonitrile, 0.1% TFA (solvent B). Separation of the three molecules began with 50% solvent A (0–2 min) followed by a gradient (2–11 min) to 5% solvent A, 95% solvent B and a short isocratic phase (11–14 min). Standard curves were generated from 25–250 μM using integrated HPLC peak intensities. Error bars are ±1 S.D. Dithranol and dithranone were directly quantified relative to standard curves; bisanthrone concentrations were deduced as the difference between the total substrate/product component and the measured amounts of dithranol and dithranone.

Monitoring Uncatalyzed Reactions Over Time—Uncatalyzed reactions between dithranol and O_2 were analyzed discontinuously over time by HPLC and continuously by UV-visible spectroscopy and O_2 consumption assays (pH 6.3 and 9.8). For HPLC, reactions were initiated by exposure of anaerobic dithranol solutions to air at the desired pH (500 μM, 20 °C). Reaction vials were gently stirred. The same reactions were monitored by UV-visible spectroscopy (100 μM dithranol, air, 20 °C) and O_2 consumption (2–20 μM dithranol, air, 20 °C), using the methods described below but excluding NMO.

Monitoring the NMO-catalyzed Reaction Over Time in the Steady State—Reactions were monitored via both UV-visible spectroscopy and O_2 consumption. For determining UV-visible spectra, 1-ml reaction solutions containing 10–200 μM dithranol (in buffer/ME at the desired pH, 20 °C) were equilibrated to air and initiated by the addition of 2–20 μM NMO (all concentrations are given as NMO subunit). For determining Michaelis-Menten parameters, the reaction was monitored in air with [dithranol] varied over 10–200 μM. The initial portion of each curve was fit to a linear equation to obtain the initial velocity (v_i, KaleidaGraph). Points were measured in triplicate and averaged (error = ±1 S.D.). Values for v_i were plotted *versus* [dithranol] and fit to Michaelis-Menten Equation 4, a derivative equation including substrate inhibition (Equation 5), or a derivative accounting for cooperative substrate interactions with dimeric NMO (h = Hill coefficient) (Equation 6),

$$v_i = V_{max}[S]/(K_M + [S]) \quad \text{(Eq. 4)}$$

$$v_i = V_{max}/(1 + K_M/[S] + [S]/K_i) \quad \text{(Eq. 5)}$$

$$v_i = V_{max}[S]^h/(K_M{}^h + [S]^h) \quad \text{(Eq. 6)}$$

For O_2 consumption, a Clark-type O_2 electrode (Yellow Springs International) in a temperature-controlled chamber (2 ml reactions, 20 °C) was used with constant stirring. The rate of background consumption of O_2 by dithranol was measured for 1 min in buffer/ME. NMO was subsequently added in catalytic amounts (2–20 μM) to initiate the reaction. Dithranol concentrations were varied from 40 to 1500 μM and [O_2] from 0.05 to 1.3 mM. The linear background rate of non-enzymatic O_2 consumption was subtracted from the rate measured in the presence of NMO. Data were plotted and fit as described above.

Effects of pH on the Steady State Reaction—Values of k_{cat} and k_{cat}/K_m(dithranol) were measured in air via O_2 electrode as a function of pH. Buffers with similar structures and a range of pK_a values (described above) were chosen and evaluated at overlapping pH values to ensure that kinetics were not buffer-dependent. The effects of incubating the enzyme at various pH values before initiating reactions *versus* adding enzyme to assay mixtures last ("pH jump") were evaluated. All buffers contained 0.3 M NaCl to minimize differences in ionic strength. Values of the Michaelis parameters were plotted *versus* pH and fit to Equation 7 to obtain values for pK_a,

$$\log(c/(1 + (10^{-x}/10^{-pK_a}))) \quad \text{(Eq. 7)}$$

where c is the difference between the minimum and maximum log k_{cat} values, and x is the pH.

Transient Kinetics of the Reaction between the NMO-Substrate Complex and O_2—Reactions were monitored using a Hi-Tech Scientific stopped-flow spectrophotometer in single mixing mode with diode array detection. The system was sealed from ambient atmosphere and rendered anaerobic by overnight incubation with protocatechuate dioxygenase and its substrate, protocatechuate (method of Ballou) (53). Protocatechuate dioxygenase and protocatechuate were flushed out of the instrument using anaerobic buffer/ME and a baseline spectrum measured (280–700 nm). All reaction solutions were made anaerobic using a double manifold Schlenk line with alternating cycles of argon gas purging and evacuation.

Concentrated solutions of the anaerobic *ES* (NMO-dithranol) complex were generated by adding 90 μM NMO (CAPS/ME (pH 9.8)) to 60 μM dithranol in an air tight tonometer. These were mixed with CAPS/ME (pH 9.8), equilibrated to various O_2 concentrations. Final O_2 concentrations after mixing with *ES* complex (measured via electrode) were 67, 140, 270, 390, and 590 μM. Progress of reaction curves were fit to single or double exponential equations, as described in the text, yielding values for k_{obs} (KinetAssyst).

Analysis of Reaction Products—The products of the NMO-catalyzed reaction were quantitatively analyzed by HPLC at various pH values. Reactions were 500 μM dithranol, air (280 μM O_2), 22 °C, with either 1 mM NMO (citrate/ME (pH 6.3), 30

min) or 50 μM NMO (CAPS/ME, pH 9.8, 10 min). Products for the uncatalyzed reactions were generated under identical conditions, but incubation times sufficient for these reactions to go to ≥90% completion were used, *i.e.* >3 half-lives: 34 h citrate/ME (pH 6.3) or 40 min CAPS/ME (pH 9.8).

Effects of Superoxide ($O_2^{\cdot-}$) Trapping on Product Distribution—Reactions and product analyses were carried out as described above but in the presence of 0, 0.5, 1.25, 2.5, or 5 mM CMH, a small molecule radical trapping agent with high specificity for $O_2^{\cdot-}$ ($k = 10^3$–10^4 M^{-1} s^{-1} (pH 7.4)), yielding $CM^{\cdot}$ and H_2O_2 (54). Alternatively, SOD (32.5 kDa, 500–5000 units/ml, 0.05–0.2 mg/reaction, Sigma) was used to enzymatically convert 2 $O_2^{\cdot-}$ to H_2O_2 and O_2 with greater steric restriction but at a substantially higher rate, $k = 6.4 \times 10^9$ M^{-1} s^{-1} (pH 7.8) (55).

Detection and Quantification of Superoxide via the CM Radical by Continuous Wave EPR Spectroscopy—$O_2^{\cdot-}$ trapping was monitored over time via the characteristic three-line EPR spectrum for $CM^{\cdot}$, a stable nitroso radical that forms following transfer of $H^{\cdot}$ from CMH to $O_2^{\cdot-}$. EPR spectroscopy was carried out at 22 °C using a Varian spectrometer: 0.2 milliwatt, 0.1 millitesla modulation amplitude, 32 ms time constant, 1-min time scans for 20–120 min. $CM^{\cdot}$ was quantified via a standard curve generated using 2,2,6,6-tetramethyl-1-piperidinyloxy (TEMPO), a stable free radical with a similar three-line EPR signal. Peak height was plotted *versus* [TEMPO] (25–300 μM TEMPO, CAPS/ME (pH 9.8)), fit to a linear equation, and the slope used to quantify unknowns.

To minimize background autocatalytic reactions between CMH/O_2 (54), EPR samples were prepared in buffers from which metals had been removed by treatment with Chelex resin (Sigma). Uncatalyzed reactions contained 200 μM dithranol, 0.1 mM diethylenetriaminepentaacetic acid as a metal chelator, air (280 μM O_2), and 1–2 mM CMH. Catalyzed reactions further contained 5 μM NMO. SOD was added to samples at 2500 units/ml, as noted. The reactions were rapidly mixed, injected into a flat cell EPR tube, and placed in the cell holder prior to measurement (manual mixing and sample loading dead time ~2–3 min).

Sequence Analysis—The ABM family was divided into subfamilies using protein network analysis (EFI-EST PFAM/Interpro Analysis). Members of each of the subfamilies containing NMO, ActVA-Orf6, and IsdG were used to generate sequence alignments (ClustalW) to identify residues conserved within each.

Author Contributions—M. M. M. carried out experiments planned collaboratively with J. L. D. R. J. U. assisted with the planning and execution of EPR experiments. J. L. D. wrote and all of the authors edited the final manuscript.

Acknowledgments—We thank Garrett Moraski and Prof. David P. Ballou, University of Michigan, for helpful discussions. The Enzyme Function Initiative (funded by National Institutes of Health Grant U54GM093342) is gratefully acknowledged for sequence network analysis tools publicly available at the Enzyme Function Initiative website (enzymefunction.org).

References

1. Que, L. Q., and Valentine, J. S. (2007) in *Biological Inorganic Chemistry: Structure and Reactivity* (Bertini, I., Gray, H. B., Stiefel, E. I., and Valentine, J. S., eds) pp. 1–40, University Science Books, Sausalito, CA
2. Fetzner, S., and Steiner, R. A. (2010) Cofactor-independent oxidases and oxygenases. *Appl. Microbiol. Biotechnol.* **86,** 791–804
3. Fetzner, S. (2012) Ring-cleaving dioxygenases with a cupin fold. *Appl. Environ. Microbiol.* **78,** 2505–2514
4. Thierbach, S., Büldt-Karentzopoulos, K., Dreiling, A., Hennecke, U., König, S., and Fetzner, S. (2012) Hydrolase-like properties of a cofactor-independent dioxygenase. *Chembiochem.* **13,** 1125–1127
5. Grocholski, T., Koskiniemi, H., Lindqvist, Y., Mäntsälä, P., Niemi, J., and Schneider, G. (2010) Crystal structure of the cofactor-independent monooxygenase SnoaB from *Streptomyces nogalater*: implications for the reaction mechanism. *Biochemistry* **49,** 934–944
6. Koskiniemi, H., Grocholski, T., Schneider, G., and Niemi, J. (2009) Expression, purification and crystallization of the cofactor-independent monooxygenase SnoaB from the nogalamycin biosynthetic pathway. *Acta Crystallogr. Sect. F Struct. Biol. Cryst. Commun.* **65,** 256–259
7. Adams, M. A., and Jia, Z. (2005) Structural and biochemical evidence for an enzymatic quinone redox cycle in *Escherichia coli*. *J. Biol. Chem.* **280,** 8358–8363
8. Sciara, G., Kendrew, S. G., Miele, A. E., Marsh, N. G., Federici, L., Malatesta, F., Schimperna, G., Savino, C., and Vallone, B. (2003) The structure of ActVA-Orf6, a novel type of monooxygenase involved in actinorhodin biosynthesis. *EMBO J.* **22,** 205–215
9. Bruice, T. C. (1984) Oxygen-flavin chemistry. *Isr. J. Chem.* **24,** 54–61
10. Massey, V. (1994) Activation of molecular oxygen by flavins and flavoproteins. *J. Biol. Chem.* **269,** 22459–22462
11. Chung, J. Y., Fujii, I., Harada, S., Sankawa, U., and Ebizuka, Y. (2002) Expression, purification, and characterization of AknX anthrone oxygenase, which is involved in aklavinone biosynthesis in *Streptomyces galilaeus*. *J. Bacteriol.* **184,** 6115–6122
12. Taguchi, T., Yabe, M., Odaki, H., Shinozaki, M., Metsä-Ketelä, M., Arai, T., Okamoto, S., and Ichinose, K. (2013) Biosynthetic conclusions from the functional dissection of oxygenases for biosynthesis of actinorhodin and related *Streptomyces* antibiotics. *Chem. Biol.* **20,** 510–520
13. Kendrew, S. G., Federici, L., Savino, C., Miele, A., Marsh, E. N., and Vallone, B. (2000) Crystallization and preliminary x-ray diffraction studies of a monooxygenase from *Streptomyces coelicolor* A3(2) involved in the biosynthesis of the polyketide actinorhodin. *Acta Crystallogr. D Biol. Crystallogr.* **56,** 481–483
14. Kendrew, S. G., Hopwood, D. A., and Marsh, E. N. (1997) Identification of a monooxygenase from *Streptomyces coelicolor* A3(2) involved in biosynthesis of actinorhodin: purification and characterization of the recombinant enzyme. *J. Bacteriol.* **179,** 4305–4310
15. Caballero, J. L., Martinez, E., Malpartida, F., and Hopwood, D. A. (1991) Organization and functions of the actVA region of the actinorhodin biosynthetic gene cluster of *Streptomyces coelicolor*. *Mol. Gen. Genet.* **230,** 401–412
16. Rafanan, E. R., Jr., Le, L., Zhao, L., Decker, H., and Shen, B. (2001) Cloning, sequencing, and heterologous expression of the elmGHIJ genes involved in the biosynthesis of the polyketide antibiotic elloramycin from *Streptomyces olivaceus* Tu2353. *J. Nat. Prod.* **64,** 444–449
17. Ye, J., Dickens, M. L., Plater, R., Li, Y., Lawrence, J., and Strohl, W. R. (1994) Isolation and sequence analysis of polyketide synthase genes from the daunomycin producing *Streptomyces* sp. strain C5. *J. Bacteriol.* **176,** 6270–6280
18. Grocholski, T., Oja, T., Humphrey, L., Mäntsälä, P., Niemi, J., and Metsä-Ketelä, M. (2012) Characterization of the two-component monooxygenase system AlnT/AlnH reveals early timing of quinone formation in alnumycin biosynthesis. *J. Bacteriol.* **194,** 2829–2836
19. Ylihonko, K., Tuikkanen, J., Jussila, S., Cong, L., and Mäntsälä, P. (1996) A gene cluster involved in nogalamycin biosynthesis from *Streptomyces nogalater*: sequence analysis and complementation of early block mutations in the anthracycline pathway. *Mol. Gen. Genet.* **251,** 113–120
20. Wu, R., Skaar, E. P., Zhang, R., Joachimiak, G., Gornicki, P., Schneewind,

O., and Joachimiak, A. (2005) *Staphylococcus aureus* IsdG and IsdI, heme-degrading enzymes with structural similarity to monooxygenases. *J. Biol. Chem.* **280,** 2840–2846
21. Streit, B. R., Kant, R., Tokmina-Lukaszewska, M., Celis, A. I., Machovina, M. M., Skaar, E. P., Bothner, B., DuBois, J. L. (2016) Time-resolved studies of IsdG identify molecular signposts along the non-canonical heme oxygenase pathway. *J. Biol. Chem.* **291,** 862–871
22. Hernández-Ortega, A., Quesne, M. G., Bui, S., Heyes, D. J., Steiner, R. A., Scrutton, N. S., and de Visser, S. P. (2015) Catalytic mechanism of cofactor-free dioxygenases and how they circumvent spin-forbidden oxygenation of their substrates. *J. Am. Chem. Soc.* **137,** 7474–7487
23. Hernandez-Ortega, A., Quesne, M. G., Bui, S., Heuts, D. P., Steiner, R. A., Heyes, D. J., de Visser, S. P., and Scrutton, N. S. (2014) Origin of the proton-transfer step in the cofactor-free (1*H*)-3-Hydroxy-4-oxoquinaldine 2,4-dioxygenase. *J. Biol. Chem.* **289,** 8620–8632
24. Steiner, R. A., Janssen, H. J., Roversi, P., Oakley, A. J., and Fetzner, S. (2010) Structural basis for cofactor-independent dioxygenation of *N*-heteroaromatic compounds at the α/β-hydrolase fold. *Proc. Natl. Acad. Sci. U.S.A.* **107,** 657–662
25. Frerichs-Deeken, U., and Fetzner, S. (2005) Dioxygenases without requirement for cofactors: identification of amino acid residues involved in substrate binding and catalysis, and testing for rate-limiting steps in the reaction of 1*H*-3-hydroxy-4-oxoquinaldine 2,4-dioxygenase. *Curr. Microbiol.* **51,** 344–352
26. Frerichs-Deeken, U., Ranguelova, K., Kappl, R., Hüttermann, J., and Fetzner, S. (2004) Dioxygenases without requirement for cofactors and their chemical model reaction: compulsory order ternary complex mechanism of 1*H*-3-hydroxy-4-oxoquinaldine 2,4-dioxygenase involving general base catalysis by histidine 251 and single-electron oxidation of the substrate dianion. *Biochemistry* **43,** 14485–14499
27. Fischer, F., Künne, S., and Fetzner, S. (1999) Bacterial 2,4-dioxygenases: new members of the α/β hydrolase-fold superfamily of enzymes functionally related to serine hydrolases. *J. Bacteriol.* **181,** 5725–5733
28. Sellmer, A., Terpetschnig, E., Wiegrebe, W., and Wolfbeis, O. S. (1998) UV/Vis and fluorescence study on anthralin and its alkylated derivatives. *J. Photochem. Photobiol. A Chem.* **116,** 39–45
29. Kralj, M., Uzelac, L., Wang, Y.-H., Wan, P., Tireli, M., Mlinarić-Majerski, K., Piantanida, I., and Basarić, N. (2015) Enhancement of antiproliferative activity by phototautomerization of anthrylphenols. *Photochem. Photobiol. Sci.* **14,** 1082–1092
30. Muller, K., Wiegrebe, W., and Younes, M. (1987) Formation of active oxygen species by dithranol, III. Dithranol, active oxygen species and lipid peroxidation *in vivo*. *Arch. Pharm.* **320,** 59–66
31. Müller, K. (1997) Antipsoriatic and proinflammatory action of anthralin. Implications for the role of oxygen radicals. *Biochem. Pharmacol.* **53,** 1215–1221
32. Müller, K. (1996) Antipsoriatic anthrones: aspects of oxygen radical formation, challenges and prospects. *Gen. Pharmacol.* **27,** 1325–1335
33. Sucharitakul, J., Phongsak, T., Entsch, B., Svasti, J., Chaiyen, P., and Ballou, D. P. (2007) Kinetics of a two-component *p*-hydroxyphenylacetate hydroxylase explain how reduced flavin is transferred from the reductase to the oxygenase. *Biochemistry* **46,** 8611–8623
34. Alfieri, A., Fersini, F., Ruangchan, N., Prongjit, M., Chaiyen, P., and Mattevi, A. (2007) Structure of the monooxygenase component of a two-component flavoprotein monooxygenase. *Proc. Natl. Acad. Sci. U.S.A.* **104,** 1177–1182
35. Palfey, B. A., Moran, G. R., Entsch, B., Ballou, D. P., and Massey, V. (1999) Substrate recognition by "password" in *p*-hydroxybenzoate hydroxylase. *Biochemistry* **38,** 1153–1158
36. Palfey, B. A., and McDonald, C. A. (2010) Control of catalysis in flavin-dependent monooxygenases. *Arch. Biochem. Biophys.* **493,** 26–36
37. Gadda, G. (2012) Oxygen activation in flavoprotein oxidases: the importance of being positive. *Biochemistry* **51,** 2662–2669
38. Roth, J. P., Wincek, R., Nodet, G., Edmondson, D. E., McIntire, W. S., and Klinman, J. P. (2004) Oxygen isotope effects on electron transfer to O_2 probed using chemically modified flavins bound to glucose oxidase. *J. Am. Chem. Soc.* **126,** 15120–15131
39. Roth, J. P., and Klinman, J. P. (2003) Catalysis of electron transfer during activation of O_2 by the flavoprotein glucose oxidase. *Proc. Natl. Acad. Sci. U.S.A.* **100,** 62–67
40. McDonald, C. A., Fagan, R. L., Collard, F., Monnier, V. M., and Palfey, B. A. (2011) Oxygen reactivity in flavoenzymes: context matters. *J. Am. Chem. Soc.* **133,** 16809–16811
41. Ukpabi, G., Takayama, S. J., Mauk, A. G., and Murphy, M. E. (2012) Inactivation of the heme-degrading enzyme IsdI by an active site substitution that diminishes heme ruffling. *J. Biol. Chem.* **287,** 34179–34188
42. Takayama, S. J., Ukpabi, G., Murphy, M. E., and Mauk, A. G. (2011) Electronic properties of the highly ruffled heme bound to the heme degrading enzyme IsdI. *Proc. Natl. Acad. Sci. U.S.A.* **108,** 13071–13076
43. Rivera, M., and Zeng, Y. (2005) Heme oxygenase, steering dioxygen activation toward heme hydroxylation. *J. Inorg. Biochem.* **99,** 337–354
44. Zeng, Y., Caignan, G. A., Bunce, R. A., Rodríguez, J. C., Wilks, A., and Rivera, M. (2005) Azide-inhibited bacterial heme oxygenases exhibit an S=3/2 (dxz,dyz)3(dxy)1(dz2)1 spin state: mechanistic implications for heme oxidation. *J. Am. Chem. Soc.* **127,** 9794–9807
45. Kahn, K., and Tipton, P. A. (1998) Spectroscopic characterization of intermediates in the urate oxidase reaction. *Biochemistry* **37,** 11651–11659
46. Colloc'h, N., el Hajji, M., Bachet, B., L'Hermite, G., Schiltz, M., Prangé, T., Castro, B., and Mornon, J. P. (1997) Crystal Structure of the protein drug urate oxidase-inhibitor complex at 2.05 angstrom resolution. *Nat. Struct. Biol.* **4,** 947–952
47. Solov'yov, I. A., and Schulten, K. (2009) Magnetoreception through cryptochrome may involve superoxide. *Biophys. J.* **96,** 4804–4813
48. Usselman, R. J., Hill, I., Singel, D. J., and Martino, C. F. (2014) Spin biochemistry modulates reactive oxygen species (ROS) production by radio frequency magnetic fields. *PLoS ONE* **9,** e93065
49. Müller, P., and Ahmad, M. (2011) Light-activated cryptochrome reacts with molecular oxygen to form a flavin-superoxide radical pair consistent with magnetoreception. *J. Biol. Chem.* **286,** 21033–21040
50. Frey, P. A., and Hegeman, A. D. (2007) *Enzymatic Reaction Mechanisms*, pp. 1–68, Oxford University Press, Oxford, UK
51. Muller, K., Gawlik, I., and Wiegrebe, W. (1995) Acidity and stability of 10-substituted 1,8-dihydroxy-9(10*H*)-anthracenones. *Arch. Pharm.* **328,** 359–362
52. Muller, K., Mayer, K., and Wiegrebe, W. (1986) Dithranol and active oxygen species, II. O_2-oxidation of dithranol to chrysazin. *Arch. Pharm. (Weinheim)* **319,** 1009–1018
53. Patil, P. V., and Ballou, D. P. (2000) The use of protocatechuate dioxygenase for maintaining anaerobic conditions in biochemical experiments. *Anal. Biochem.* **286,** 187–192
54. Dikalov, S. I., Kirilyuk, I. A., Voinov, M., and Grigor'ev, I. A. (2011) EPR detection of cellular and mitochondrial superoxide using cyclic hydroxylamines. *Free Radic. Res.* **45,** 417–430
55. Gray, B., and Carmichael, A. J. (1992) Kinetics of superoxide scavenging by dismutase enzymes and manganese mimics determined by electron spin resonance. *Biochem. J.* **281,** 795–802
56. Ballou, D., Palmer, G., and Massey, V. (1969) Direct demonstration of superoxide anion production during oxidation of reduced flavin and of its catalytic decomposition by erythrocuprein. *Biochem. Biophys. Res. Commun.* **36,** 898–904
57. Kemal, C., and Bruice, T. C. (1979) Transfer of O_2 from a 4a-hydroperoxyflavin anion to a phenolate ion. A flavin-catalyzed dioxygenation reaction. *J. Am. Chem. Soc.* **101,** 1635–1638
58. Kemal, C., Chan, T. W., and Bruice, R. C. (1977) Reaction of $^3O_2$ with dihydroflavins. 1. *N*3,5-dimethyl-1,5-dihydrolumiflavin and 1,5-dihydroisoalloxazines. *J. Am. Chem. Soc.* **99,** 7272–7286
59. Roth, J. (2009) Oxygen isotope effects as probes of electron transfer mechanisms and structures of activated O_2. *Acc. Chem. Res.* **42,** 399–408
60. Palfey, B., Frederick, K., Moran, G., Entsch, B., Ballou, D., and Massey, V. (2000) Proton movements control the reduction of FAD in *p*-hydroxybenzoate hydroxylase. *Biochemistry* **39,** 1556–1557

Monooxygenase Substrates Mimic Flavin to Catalyze Cofactorless Oxygenations

Melodie M. Machovina, Robert J. Usselman and Jennifer L. DuBois

J. Biol. Chem. 2016, 291:17816-17828.
doi: 10.1074/jbc.M116.730051 originally published online June 15, 2016